Modeling events of sea-surface variability using spectral nudging in an eddy permitting model of the northeast Pacific Ocean

Michael W. Stacey,[1] Jennifer Shore,[1] Daniel G. Wright,[2] and Keith R. Thompson[3]

Received 2 September 2005; revised 12 January 2006; accepted 13 March 2006; published 28 June 2006.

[1] Eddies are an important part of the current system that hugs the coasts of British Columbia and Alaska. The ability of "spectral nudging" to improve the eddy statistics determined from model simulations of this current system is investigated. Spectral nudging differs from standard nudging in that only specified frequency and wave number bands of the simulated potential temperature and salinity fields are nudged toward the observed climatology. Therefore the simulated eddy field can develop and evolve with time while the model is prevented from drifting far from the observed climatology. The Parallel Ocean Program (POP) is used to do the simulations, with 0.25° horizontal resolution and 23 vertical levels. The simulated standard deviation and skewness fields for the sea surface height are compared with those estimated from ten years of TOPEX/Poseidon altimetry observations. This comparison shows that spectral nudging allows the model to simulate the eddy statistics of the current system with significantly more accuracy than when the nudging is not used.

Citation: Stacey, M. W., J. Shore, D. G. Wright, and K. R. Thompson (2006), Modeling events of sea-surface variability using spectral nudging in an eddy permitting model of the northeast Pacific Ocean, *J. Geophys. Res.*, *111*, C06037, doi:10.1029/2005JC003278.

1. Introduction

[2] Although the northeast Pacific Ocean has received less attention from numerical modelers than many other ocean environments, there have been a number of numerical studies concentrating on the tidal, wind-driven and density-driven aspects of the circulation in the northeast Pacific basin and its coastal ocean [e.g., *Cummins and Oey*, 1997; *Foreman et al.*, 2000; *Masson and Cummins*, 2000; *Cummins et al.*, 2000, 2001; *Murray et al.*, 2001; *Masson*, 2002; *Hermann et al.*, 2002; *Di Lorenzo et al.*, 2005]. In this paper, simulations of the North Pacific Ocean with emphasis on the northeast Pacific (Lat.: 40–60°N; Long.: 140–240°W) are discussed. These simulations differ significantly from those of previous studies in that a recently developed nudging technique [*Thompson et al.*, 2006] is used to avoid model drift from observed climatology. It is found that when this "spectral" nudging technique is used, a numerical model's ability to simulate the sea-surface height variability in the Gulf of Alaska improves. One of our long-term goals is to improve our forecasts of the evolution of specific events (e.g., eddies) in the northeast Pacific. In order to do that however, a model must first be able to reproduce the basic character of the variability in the eddy field, and spectral nudging is a technique that can be used to improve a model's ability to do that.

[3] The Parallel Ocean Program (POP) is used to do the simulations. The POP was developed at Los Alamos [*Maltrud et al.*, 1998; *Smith et al.*, 2000] and was chosen in part because it has been coded to run efficiently on parallel computer systems like that at the High Performance Computing Virtual Laboratory (HPCVL; http://hpcvl.org) that we have used to produce the simulations presented here.

[4] Version 1.8 of the POP has been modified [*Thompson et al.*, 2006; D. G. Wright et al., Assimilating long-term hydrographic information into an eddy-permitting model of the North Atlantic, submitted to *Journal of Geophysical Research*, 2006] so that the simulated climatology of the potential temperature θ and salinity S fields can be nudged toward the observed "climatology." Nudging is required to avoid model drift and bias because of imperfections in the model dynamics and the specified forcing fields. Such imperfections are inevitable with the finite resolution imposed by the practicalities of limited computer resources. Standard nudging prevents the total simulated θ and S fields from drifting far from climatology, and so the formation of eddies in the simulation is strongly suppressed or even eliminated. Therefore, if one wants to simulate the eddy activity of a current system, standard nudging is not useful. However, it is desirable to prevent excessive drift of the model's climatology when examining eddy properties, particularly since eddies extract potential and/or kinetic energy from the mean state through baroclinic and/or barotropic instabilities. Clearly, errors in the mean state will be reflected in both eddy generation and propagation. *Thompson et al.* [2006] have developed a technique by which only the θ and

[1]Department of Physics, Royal Military College of Canada, Kingston, Ontario, Canada.
[2]Ocean Circulation Section, Bedford Institute of Oceanography, Dartmouth, Nova Scotia, Canada.
[3]Department of Oceanography, Dalhousie University, Halifax, Nova Scotia, Canada.

0148-0227/06/2005JC003278

S variability in particular frequency bands is nudged toward the corresponding observed conditions. Using this method, the mean and "low" frequency components of the simulated θ and S fields can be nudged toward climatology while the "high" frequency eddy component of the simulated fields is allowed to evolve according to the model dynamics.

[5] Eddies (and eddy trains) frequently form in the current system that hugs the coasts of British Columbia and Alaska [*Thomson and Gower*, 1998; *Crawford et al.*, 2000], and instability of the mean flow is considered to be an important mechanism by which these eddies form [*Thomson and Gower*, 1998]. Accurate forecasts of the circulation there will require a model that can accurately reproduce the eddy field. By comparing the simulated sea-surface height variability to that obtained from satellite altimetry observations, it will be shown that the model simulation improves when spectral nudging is used. Altimetry has been used to do the validations because its coverage in the northeast Pacific is much more complete than that of any other set of observations.

[6] Skewness fields will also be calculated from the observed altimetry and the simulated sea-surface displacement. Skewness gives a measure of the direction of rotation of the eddies [*Thompson and Demirov*, 2006].

2. Model

[7] The POP is an adaptation of the Modular Ocean Model (MOM) developed at the GFDL that has been coded to run efficiently on parallel computer systems. It uses a B-grid with fixed geopotential levels, and also includes implicit treatments of the free surface and Coriolis terms [*Smith et al.*, 1992; *Dukowicz and Smith*, 1994] and implementation of pressure averaging [*Brown and Campana*, 1978] to increase computational efficiency.

[8] The entire model domain is shown in Figure 1. The domain is essentially the North Pacific, and the open boundary is near the equator. This domain was used so that the open boundary would be located far from our region of primary interest, shown in Figure 2 and to provide a first look at the model results in the rest of the North Pacific.

[9] The bathymetry, shown in Figure 2, is derived from the *Smith and Sandwell* [1997] database but has been smoothed in the northeast Pacific. The bathymetry was smoothed because the spatial grid of the model was not very fine and it was felt that the small-scale variability in the bathymetry might cause unrealistic numerical variability in the simulated circulation [e.g., *Penduff et al.*, 2002]. (The bathymetry in the northeast sector of the model is also shown in Figure 3.) The horizontal grid resolution was 0.25° in longitude but variable in latitude so that the grid cells remain approximately square. There were 23 vertical levels (Table 1). (Simulations with a horizontal resolution of 0.5° in longitude were also tried but found to be quite poor.) Other models of the region have used finer resolution. For example, *Murray et al.* [2001], and *Di Lorenzo et al.* [2005] used horizontal resolutions of 1/16° and about 8 km respectively.

[10] Also shown in Figure 2 is the domain over which the simulations and observations were quantitatively compared. This limited domain was chosen because we are interested in doing the comparisons where there is strong eddy formation. Away from this region, the model tends to underestimate the sea-surface height variability whether spectral nudging is used or not.

[11] Unresolved horizontal mixing processes are represented by biharmonic mixing with the horizontal viscosity coefficient equal to $-9.8 \times 10^{18}\mathrm{cm}^4\mathrm{s}^{-1}$ at the southern boundary and varying with the cube of the grid cell width and the diffusivity equal to one eighth of the viscosity coefficient. Vertical mixing is represented by the KPP approximation [*Large et al.*, 1994] with the double-diffusion contribution neglected.

[12] The surface momentum flux is specified according to monthly climatological data [*da Silva et al.*, 1994]. For the heat flux, we use DaSilva's estimate of the climatological flux plus a restoring term determined by model-data discrepancies analogous to the approach of *Barnier et al.* [1995]. This approach maintains realistic surface fluxes as model-data misfits tend to zero. Persistent misfits are not an essential aspect of the solution as in the standard restoring approach when surface values are restored toward climatological conditions and determination of an appropriately adjusted restoring temperature, as in the approach suggested by *Haney* [1971], is not required. On the other hand, the virtual surface salt flux is determined solely by restoring to climatological conditions but annual mean misfits are treated specially as discussed below. In each case, the observational estimates of climatological conditions are estimated by linearly interpolating between monthly estimates.

[13] The restoring terms used in the determination of both heat and virtual salt fluxes are composed of two parts. The first part is a term that pulls the annual mean component of the model field toward the corresponding observational estimate with a short relaxation timescale of just 10 days. The second part of each restoring term pulls instantaneous surface values toward observational estimates with the longer relaxation timescale of 50 days. By using this approach, the model's surface climatology is strongly constrained to agree with observations but deviations from the climatology are still permitted over eddy timescales.

[14] To crudely account for water mass changes that occur outside of the model domain, "sponge layers" are included adjacent to the northern and southern boundaries. Within these layers, the inverse of the restoring time varies linearly from 1 day^{-1} to 0 day^{-1} from the open boundary to 2° inside of the model domain.

3. Data

[15] As noted above, monthly climatological data [*da Silva et al.*, 1994] are used to specify the surface momentum flux and the initial estimate of the surface heat flux. The θ and S fields are from monthly climatological Levitus data [*Levitus et al.*, 1994; *Levitus and Boyer*, 1994] except in our region of interest (Figure 2) where more complete observations obtained from the Institute of Ocean Sciences (IOS) in Sidney British Columbia (B. Crawford, personal communication, 2004) were used. These high-resolution observations of temperature and salinity were available only as summer and winter averages and hence were averaged to produce a mean signal. The results were then interpolated to the upper northeast part of the grid used for the POP simulations. The

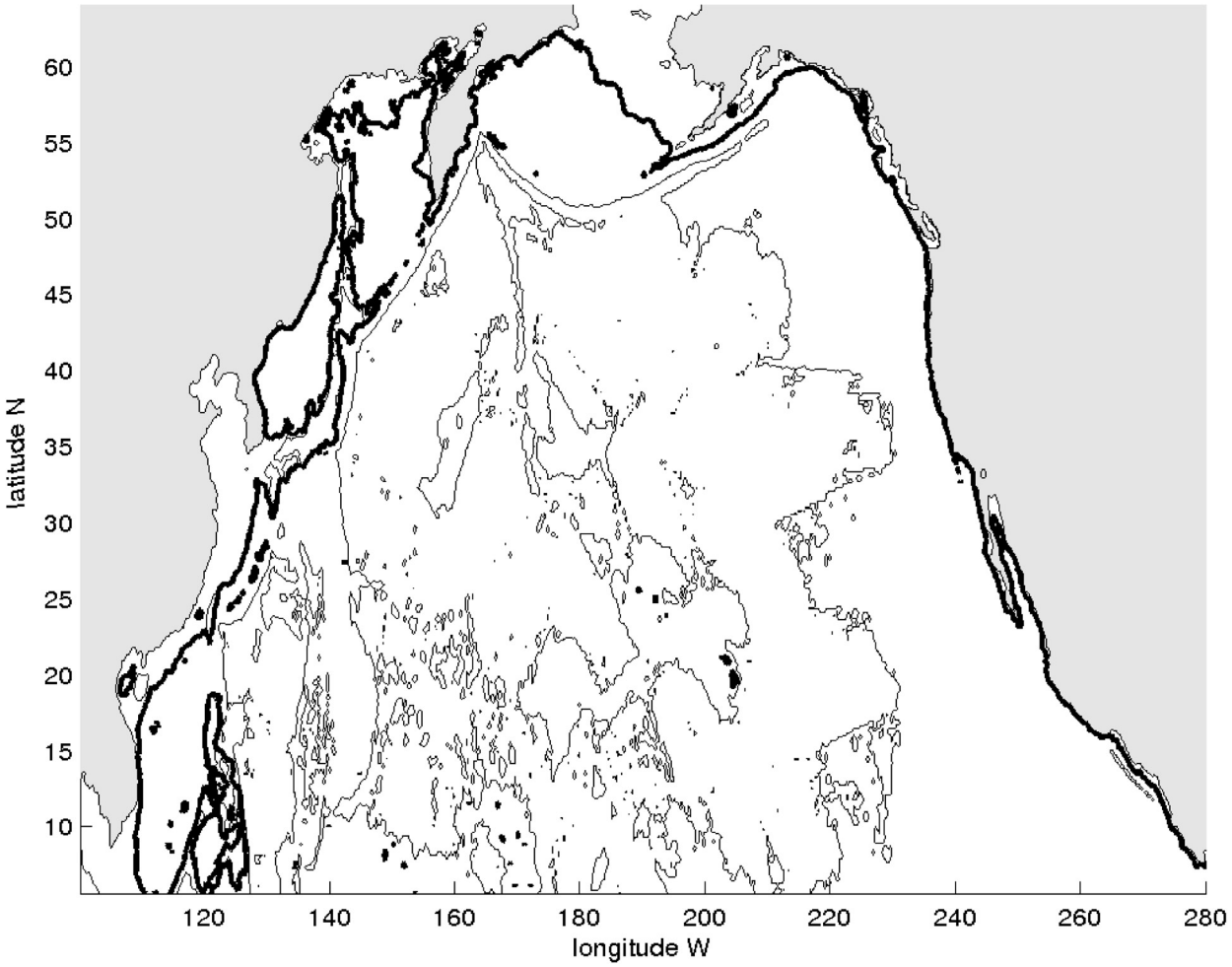

Figure 1. Depth contours at 10, 200 and 4800 m for the entire model domain. The 200 m contour is shown as a thick bold line. Land surfaces are shaded.

interpolated results were then used to replace the annual mean component of the Levitus data in that region. Specifically, the mean component of the Levitus data was computed and removed leaving only the Levitus monthly anomaly in this subdomain. The higher-resolution IOS mean observations were then added to the Levitus monthly anomaly and the resulting temperature and salinity fields were blended with the remaining Levitus data along the edges of that subdomain. The model was initialized in January with the Levitus/IOS climatology, and was spun up from rest.

[16] Ten years of TOPEX/Poseidon altimetry data (obtained from Dr. Josef Cherniawsky at IOS), taken between 23 September 1992 and 11 August 2002, were used to calculate the basic statistics of the sea-surface height for comparison with the simulations. There were 62 satellite tracks and the repeat period for each track was about 10 days. Time series of sea-surface height were constructed for each observation location [denoted location i in equations (3) and (4)], and each time series was least squares fitted to the local mean and the constituents Sa (period = 365.2 days) and Ssa (period = 182.6 days). Time series of sea-surface height anomaly were then constructed for each location by subtracting the mean, Sa and Ssa from each sea-surface height time series. Note that because Sa and Ssa were removed, the annual and seasonal cycles were largely removed.

4. Spectral Nudging

[17] Spectral nudging is an approach introduced by *Thompson et al.* [2006] to avoid drift on long timescales and large space scales while allowing higher frequency variability and small-scale details to evolve according to the model dynamics. In this section we provide a very brief review of the simple form of spectral nudging used here.

[18] In the standard robust diagnostic approach [e.g., *Sarmiento and Bryan*, 1982], one adds terms in the temperature and salinity equations that are proportional to the difference between the observational estimates of the climatology and the instantaneous model values to maintain model values near the climatological estimates. A significant drawback of this approach is that strong restoring is required to obtain a close match between the model and the

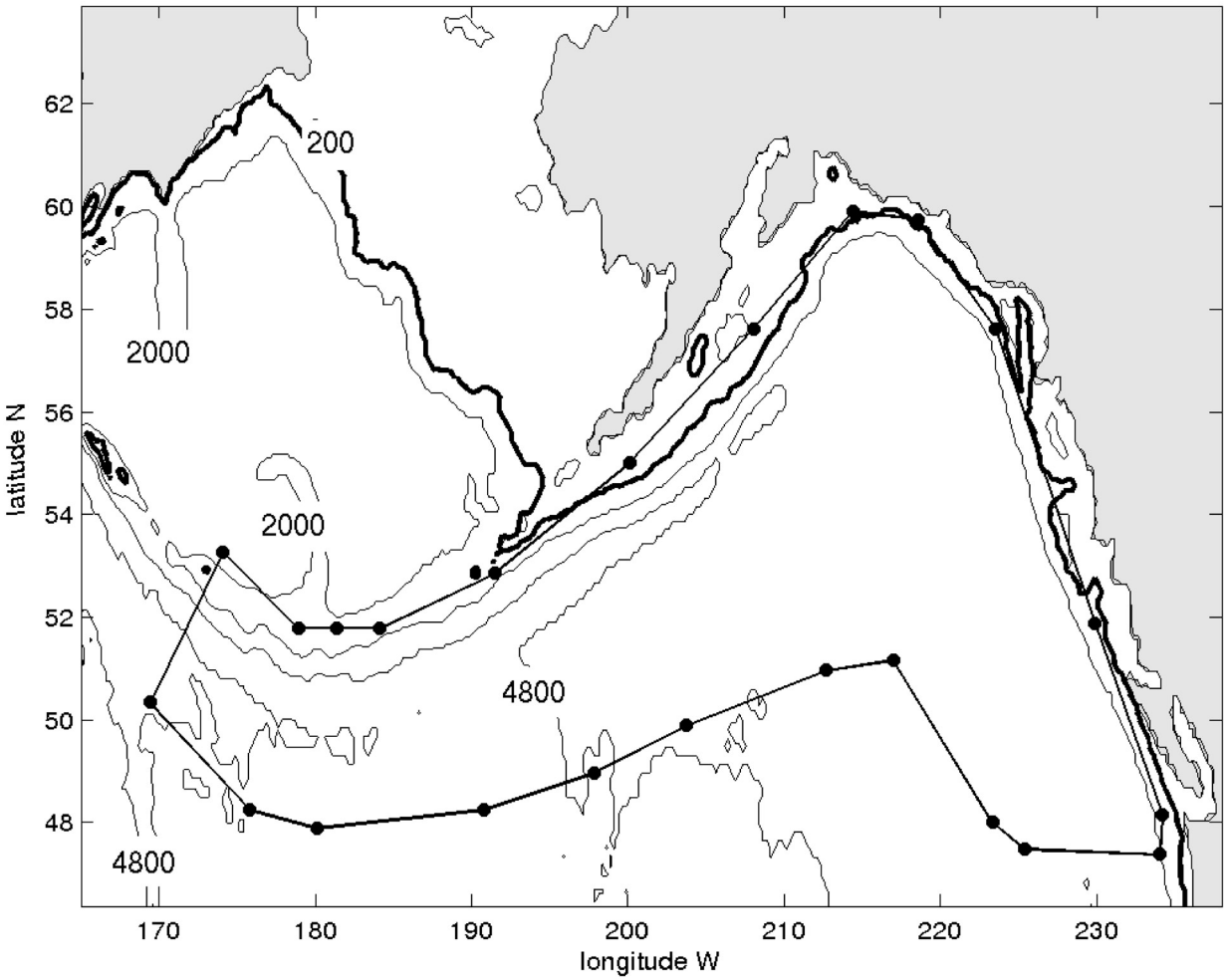

Figure 2. Subdomain of interest, the northeast Pacific Ocean. The domain over which MRSE and RME (see expressions (3) and (4) and Table 2) are calculated is contained within the solid line on which there are the solid circles. The same limited domain is used in producing the scatterplots in Figure 4.

observed climatologies, and this has the effect of suppressing variability that is not represented by the climatological data [e.g., *Woodgate and Killworth*, 1997].

[19] The essence of the approach introduced by *Thompson et al.* [2006] is to replace the nudging term, $\Delta = \gamma(x^{cl} - x)$, by $\langle\tilde{\Delta}\rangle$, where the tilde represents a temporal filter and the angled brackets represent a spatial filter, so that only selected frequencies and length scales remain in the nudging terms. The properties of both the temporal and spatial filters can vary over the model domain if desired.

[20] In this paper, we have used the seasonal filter described by *Thompson et al.* [2006] to filter the differences between the observed climatology and the model before nudging the model. In essence this is achieved by fitting the form $\alpha_0 + \alpha_1 \cos(\omega\, t + \phi)$, where $\omega = 2\pi/365$ days and α_0, α_1 and ϕ are constants in time determined independently for each grid point in the model, to the difference between the observed and model fields. (One of the attractions of this filter is the zero phase lag of the filter response at the mean and annual cycle. The details are given in the appendix of *Thompson et al.* [2006].) This fit was done recursively as the run progressed over a sliding window that extends backward in time over 10 years or the time since the run was initiated, whichever is shorter; over the final 10 years used for our intercomparisons with observations, the fit is done over the preceding 10 year interval. The parameter α_0 was then spatially filtered to remove spatial scales less than 50 km. Although it might be possible to filter out eddy variability from the nudges using spatial smoothing, we have not attempted to do this. Instead, we have used the temporal filter to achieve this result. The spatial smoothing is included primarily to allow greater freedom for the model state to adjust at small spatial scales within the frequency bands constrained by the nudges. This is desirable because of small-scale errors in the topography that are introduced by the model discretization.

[21] The total nudge is given by:

$$\left\langle\tilde{\Delta}\right\rangle = \frac{2\Delta t}{\tau}\left\langle\bar{x}^{cl} - \bar{x}\right\rangle = \frac{2\Delta t}{\tau}\langle\alpha_0\rangle, \tag{1}$$

where τ = 20 *days*. Note that both the mean and annual cycle of the model-data misfits were estimated but we

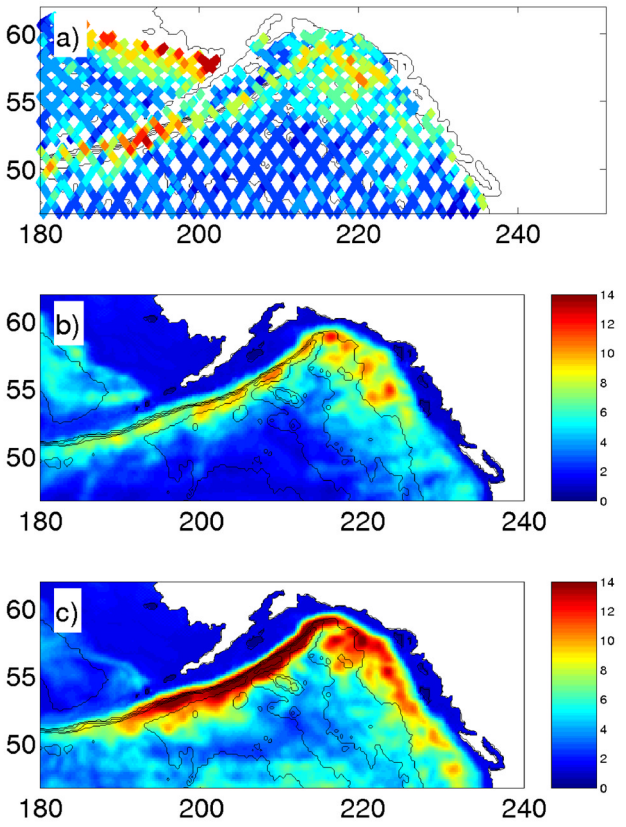

Figure 3. Standard deviation for (a) the satellite altimetry, (b) the prognostic simulation, and (c) the simulation that uses spectral nudging.

choose to nudge only the mean state (indicated by an overbar) in the present study. The model state is free to adjust over the restoring timescale of 20 days even within the frequency bands constrained by the nudging. This timescale is short enough to strongly constrain scales in excess of 200 km but long enough to avoid overconstraining the model's mean state at the more poorly determined small scales. The inclusion of spatial filtering of the nudges reduces the sensitivity to a reduction in τ but this effect has not been examined in detail. The nudges are updated once per day and the determination and addition of the nudging terms to the tracer equations increases CPU load by less than 25%, making this a very efficient data assimilation scheme. Since the nudges vary only slowly in time, they could be updated even less frequently to allow for the use of more sophisticated spatial filters without increasing the CPU requirements. This possibility warrants investigation but has not been considered here.

5. Results

[22] For each simulation, the model was spun up from rest over twenty years of simulation time. The last ten years of each simulation were used to calculate the standard deviation and the skewness of the sea-surface height for comparison with the same fields calculated from the ten years of altimetry observations.

[23] The standard deviation gives a simple measure of the magnitude of the sea-surface height variability, and the skewness, defined as:

$$skewness(i) = \frac{\frac{1}{M}\sum_{j=1}^{M}\left(\eta_j^i - \overline{\eta^i}\right)^3}{\left[\frac{1}{M}\sum_{j=1}^{M}\left(\eta_j^i - \overline{\eta^i}\right)^2\right]^{3/2}} = \frac{\frac{1}{M}\sum_{j=1}^{M}\left(\eta_j^i - \overline{\eta^i}\right)^3}{[\sigma^i]^3} \quad (2)$$

gives a measure of the predominant direction of rotation as well as the intensity and frequency of the eddies that are formed. For the model, the $skewness(i)$ is the skewness at model point i, M is the number of model data points in the 10 year time series at model point i ($M = 350$), η_j^i is the sea-surface height at location i at time j, $\overline{\eta^i}$ is the time averaged sea-surface height at location i, and σ^i is the standard deviation in the sea-surface height at location i. For the altimetry observations, i denotes the location of an observation point and j denotes an observation from the time series constructed for the location i. A positive (negative) skewness implies a bias toward anticyclonic (cyclonic) rotation, since a positive (negative) height anomaly implies anticyclonic (cyclonic) rotation. Both *Thomson and Gower* [1998] and *Crawford et al.* [2000] found the observed eddies in this region to be predominantly anticyclonic.

[24] Figure 3 shows the standard deviation fields for the northeast Pacific, for the altimetry observations (Figure 3a) and for the prognostic (nonnudged) (Figure 3b) and nudged (Figure 3c) simulations. The difference between the two simulated fields is easy to see by eye. (Simulations that used standard nudging with no spatial or temporal filtering of the nudges were also considered, but results are not shown here.

Table 1. Layer Thicknesses for the Model[a]

Number	Layer Thickness, m
1	10
2	10
3	15
4	20
5	20
6	25
7	35
8	50
9	75
10	100
11	150
12	200
13	275
14	350
15	415
16	450
17	500
18	500
19	500
20	500
21	500
22	500
23	500

[a]The top and bottom of each layer is a vertical velocity (w) point. Midway between each layer, and below the w point, is a potential temperature, salinity, pressure (θ, S, p) point; midway between each layer, and offset, is a horizontal velocity point.

Table 2. MRSE and RME (See Expressions (3) and (4)) for the Standard Deviation and the Skewness[a]

	Standard Deviation, %		Skewness, %	
	MRSE	RME	MRSE	RME
Prognostic	20.4	−37.7	16.6	135
Nudged	14.6	−7.1	15.5	114

[a]MRSE and RME were calculated using the domain shown in Figure 2. For the skewness, only values with magnitude of 0.75 or greater were considered.

This approach was found to suppress the eddy field almost completely resulting in very unrealistic standard deviation fields.)

[25] Table 2 shows the average of the squared relative difference between the altimetry and simulated standard deviation at each model point (MRSE), and also the relative difference in the spatially averaged standard deviations (RME). (The model values were interpolated to the location of the altimetry observations for these calculations.) Each average was calculated over the limited subdomain shown in Figure 2. As noted earlier, this subdomain includes the region where eddy activity predominates. MRSE and RME are defined here as:

$$MRSE = \frac{1}{N}\sum_{i=1}^{N}\left[\frac{\sigma_M^i - \sigma_O^i}{\sigma_O^i}\right]^2 \tag{3}$$

and

$$RME = \frac{\frac{1}{N}\sum_{i=1}^{N}\sigma_M^i - \frac{1}{N}\sum_{i=1}^{N}\sigma_O^i}{\frac{1}{N}\sum_{i=1}^{N}\sigma_O^i} \tag{4}$$

where N is the number of points (=5880) in the limited spatial domain, σ_M^i is the model standard deviation interpolated to observation point i, calculated from the last ten years of the twenty year simulation, and σ_O^i is the altimetry standard deviation at location i, calculated from the ten years of data. The values in Table 2, particularly for RME, show that the nudging has indeed produced a simulation with more accurate sea-surface height variability. The implication is that spectral nudging is a useful technique to use when simulating the circulation of the northeast Pacific.

[26] Comparing the contours in Figure 3 by eye, it appears that the eddy activity in the immediate shelf-slope region is overestimated by the nudged run. (The prognostic run, as the statistics in Table 2 confirms, underestimates the eddy activity.) It is perhaps worth emphasizing here that the eddy field that one obtains when using spectral nudging can depend significantly on the observed climatology. We have tried a number of somewhat different climatologies (see section 6) and each climatology produces a somewhat different eddy field. Given the statistical measures and the subdomain we have chosen, the climatology described in section 3, with the smoothed bathymetry, gives the most accurate results. Modifying the subdomain and/or the statistical measures (and/or the bathymetry, plus other possible modifications not tried by us) could change which climatology is considered to give the most accurate results. Regardless however, we have shown here is that it is possible, when using spectral nudging, to simulate an active eddy field while at the same time holding the simulated climatology close to that of the observed climatology. Since the energy for the eddy field is derived from the mean fields, spectral nudging can therefore result in more accurate simulated eddy fields, subject of course to the observed climatology itself being accurate.

[27] Figure 4 shows scatterplots of the observed and modeled standard deviation for the prognostic (Figure 4a) and nudged (Figure 4b) runs. The prognostic run clearly tends to underestimate the magnitude of the sea-surface variability. For the nudged run, the simulation produces standard deviations for which there is a more even distribution of underestimated and overestimated values. It is the overestimated values that give the impression that the nudged run (Figure 3c) may be overestimating the intensity of the eddy field. By decreasing the domain over which the statistics are calculated to include only the slope region, we would obtain a domain-averaged standard deviation that was larger than that of the observations. Conversely, by increasing the domain we would obtain a standard deviation that was smaller than that of the observations.

[28] Figure 5 shows the skewness fields for the northeast Pacific, for the altimetry observations (Figure 5a) and for the prognostic (Figure 5b) and nudged (Figure 5c) simulations. The mostly positive values for the observed skewness reflects the fact, as previously found [e.g., *Thomson and Gower*, 1998; *Crawford et al.*, 2000], that the eddies are predominantly anticyclonic. Both the prognostic and nudged simulations also show mostly positive values for the skewness, and their skewness fields are visually more alike than their standard deviation fields. Note however that as one proceeds west along the south coast of Alaska, the skewness field of the nudged run exists as a positive band hugging the shelfbreak for a longer distance than does that of the prognostic run, in closer agreement with the skewness field calculated from the observations.

[29] Table 2 also shows the MRSE and RME values for the skewness. They are the same as expressions (3) and (4) but with the skewness replacing the standard deviation. In this case it is not clear that the nudged run is producing the more accurate result. Both simulations are producing primarily anticyclonic eddies, given the mostly positive values for the skewness, but one field is not unambiguously more accurate than the other. In calculating MRSE and RME, only skewness values with magnitudes greater then 0.75 were included. Otherwise, the smallest skewness values dominate the calculation of MRSE, and values greater than 6000 are obtained. (The skewness scatterplots for the prognostic and nudged runs look very similar.)

6. Summary and Conclusions

[30] An eddy permitting ocean model that uses spectral nudging can simulate the sea-surface height variability of the current system that hugs the coasts of British Columbia and Alaska with more accuracy than a prognostic model with the same 0.25° horizontal spatial resolution. Standard nudging suppresses the eddy field almost completely and results in a very poor simulation of the sea-surface height

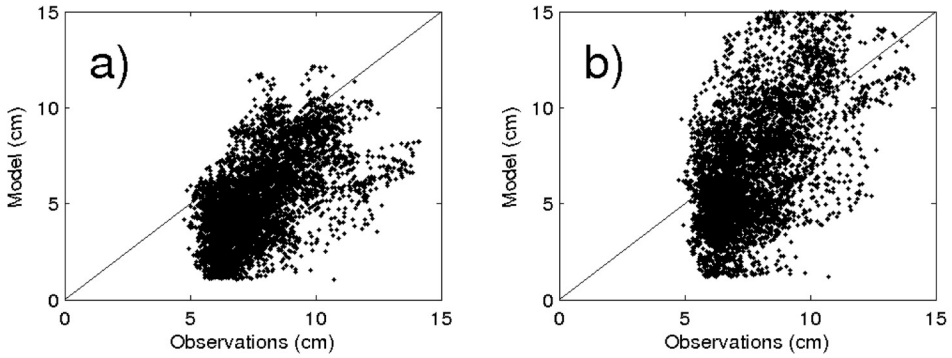

Figure 4. Scatterplots of the standard deviations for (a) the satellite altimetry and prognostic simulation and (b) the satellite altimetry and the simulation that uses spectral nudging.

variability, but spectral nudging allows the eddies to develop while holding the mean θ and S fields close to the observed climatology, thereby providing the eddy field with a source of energy from the mean field that does not degrade over time. These results support the idea that spectral nudging can be a useful tool to use when simulations requiring accurate reproduction of eddy variability are needed, but for which very fine resolution is not practical. Forecasts requiring accurate simulation of the eddy field and for which good knowledge of the mean scalar fields is available should benefit from the use of spectral nudging.

[31] The standard deviation field of the sea-surface height variability is better simulated when spectral nudging is used. The prognostic simulation produces a variability field that is too weak because the θ and S fields drift from climatology over time and provide a smaller source of energy for the variability than does the nudged case.

[32] The skewness fields, which give a measure of the predominant direction of rotation of the eddies, show that both for the observations and the simulations, anticyclonic rotation predominates. Both the prognostic and the nudged simulations produce primarily anticyclonic rotation.

[33] Note that the wind stress and buoyancy forcing terms applied to the model are each determined from climatological data sets so that all deviations from the annual cycle must be due to nonlinear effects. In particular, the eddy variability produced by the model must be almost entirely determined by nonlinearities in the model.

[34] Model runs were done using just the Levitus observed climatology (i.e., not inserting the climatology for the northeast Pacific provided by IOS), using the climatology provided by IOS for the northeast Pacific but without the monthly Levitus anomalies added, and with smoothed and unsmoothed bathymetry. Smoothing the bathymetry had relatively little effect on the prognostic runs. Including the Levitus anomalies with the IOS means had only a small effect on the simulation. For most but not all of the nudged runs, smoothing the bathymetry tended to improve the simulations, meaning that the standard deviation fields were closer to those calculated from the altimetry observations. For all of the combinations of climatology and bathymetry that were tried however, the nudged runs were more accurate than the prognostic runs. Unsmoothed bathymetry was not tried with the climatology used to produce the results presented in this paper, but it was tried using the IOS data within the subdomain but without the Levitus anomalies added. Then, the prognostic model with unsmooothed bathymetry gave (MRSE = 17.7%; RME = −30.7%), and with smoothed bathymetry gave (MRSE = 18.5%; RME = −34.3%). The nudged run with unsmoothed bathymetry gave (MRSE = 17.2%; RME = 3.0%), and with smoothed bathymetry gave (MRSE = 13.7%; RME = −9.0%).

[35] We are continuing to examine the dynamics of the eddy field that is generated along the coasts of British Columbia and Alaska. Also, because the model domain

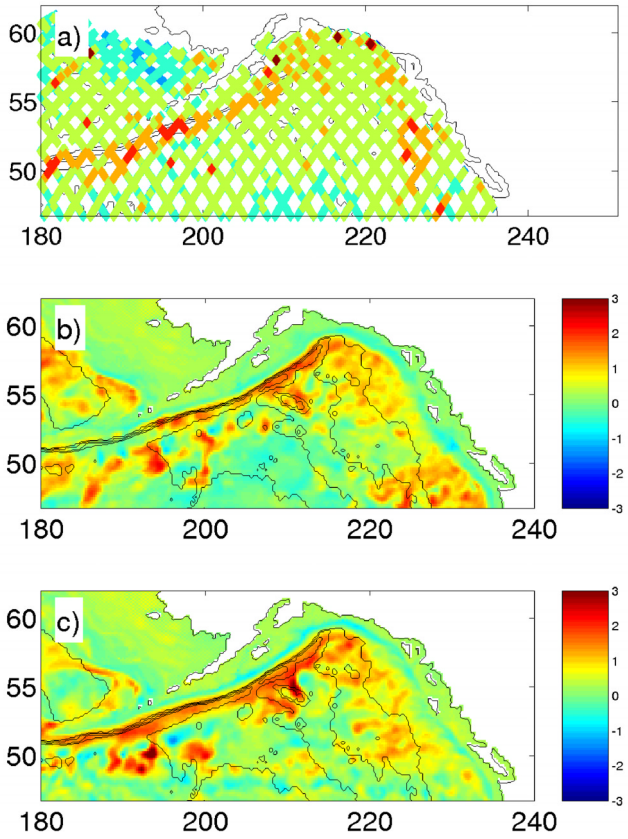

Figure 5. Skewness for (a) the satellite altimetry, (b) the prognostic simulation, and (c) the simulation that uses spectral nudging.

includes the entire North Pacific Ocean, the influence of spectral nudging on other aspects of the North Pacific circulation (e.g., the Kuroshio current) will be investigated in the future. The possibility of using spectral nudging in studies of interannual and interdecadal variability will be considered, but this will require much longer model simulations so that the bandwidth of the nudged frequencies can be greatly reduced in comparison to the present study.

[36] **Acknowledgments.** This research has been supported by a grant from the Canadian Foundation for Climate and Atmospheric Research. The High Performance Computing Virtual Laboratory (HPCVL; http://www.hpcvl.org) was used to perform the simulations. We thank Josef Cherniawsky for supplying us with the satellite data and Bill Crawford for supplying us with the improved climatology for the northeast Pacific. Keith Thompson wishes to thank NSERC for its support.

References

Barnier, B., L. Siefridt, and P. Marchesiello (1995), Thermal forcing for a global ocean circulation model using a three-year climatology of ECMWF analyses, *J. Mar. Syst.*, *6*, 363–380.

Brown, J. A., and K. A. Campana (1978), An economical time-differencing system for numerical weather prediction, *Mon. Weather Rev.*, *106*, 1125–1136.

Crawford, W. R., J. Y. Cherniawsky, and M. G. G. Foreman (2000), Multi-year meanders and eddies in the Alaskan Stream as observed by TOPEX/Poseidon altimeter, *Geophys. Res. Lett.*, *27*, 1025–1028.

Cummins, P. F., and L.-Y. Oey (1997), Simulation of barotropic and baroclinic tides off Northern British Columbia, *J. Phys. Oceanogr.*, *27*, 762–781.

Cummins, P. F., D. Masson, and M. G. G. Foreman (2000), Modeling diurnal tides and currents off Vancouver Island, *J. Phys. Oceanogr.*, *30*, 15–30.

Cummins, P. F., J. Y. Cherniawsky, and M. G. G. Foreman (2001), North Pacific internal tides from the Aleutian Ridge: Altimeter observations and modeling, *J. Mar. Res.*, *59*, 167–192.

da Silva, A. M., C. C. Young, and S. Levitus (1994), *Atlas of Surface Marine Data 1994*, vol. 1, *Algorithms and Procedure*, *NOAA Atlas NESDIS 6*, 83 pp., U.S. Dep. of Commer., Washington, D. C.

Di Lorenzo, E., M. G. G. Foreman, and W. R. Crawford (2005), Modeling the generation of Haida eddies, *Deep Sea Res., Part II*, *52*, 853–873.

Dukowicz, J. K., and R. D. Smith (1994), Implicit free-surface method for the Bryan-Cox-Semtner ocean model, *J. Geophys. Res.*, *99*, 7991–8014.

Foreman, M. G. G., W. R. Crawford, J. Y. Cherniawsky, R. F. Henry, and M. R. Tarbotton (2000), A high resolution assimilating tidal model for the northeast Pacific Ocean, *J. Geophys. Res.*, *105*, 28,629–28,652.

Haney, R. L. (1971), Surface thermal boundary condition for ocean circulation models, *J. Phys. Oceanogr.*, *1*, 241–248.

Hermann, A. J., D. B. Haidvogel, E. L. Dobbins, and P. J. Stabeno (2002), Coupling global and regional circulation models in the coastal Gulf of Alaska, *Prog. Oceanogr.*, *53*, 335–367.

Large, W. G., J. C. McWilliams, and S. C. Doney (1994), Oceanic vertical mixing: A review and a model with non-local boundary layer parameterization, *Rev. Geophys.*, *32*(4), 363–403.

Levitus, S., and T. P. Boyer (1994), *World Ocean Atlas 1994*, vol. 4, *Temperature*, *NOAA Atlas NESDIS 4*, 129 pp., U.S. Dep. of Commer., Washington, D. C.

Levitus, S., R. Burgett, and T. P. Boyer (1994), *World Ocean Atlas 1994*, vol. 3, *Salinity*, *NOAA Atlas NESDIS 3*, 111 pp., U.S. Dep. of Commer., Washington, D. C.

Maltrud, M. E., R. D. Smith, A. J. Semtner, and R. C. Malone (1998), Global eddy-resolving ocean simulations driven by 1985–1995 winds, *J. Geophys. Res.*, *103*, 30,825–30,853.

Masson, D. (2002), Deep water renewal in the Strait of Georgia, *Estuarine Coastal Shelf Sci.*, *54*, 115–126.

Masson, D., and P. F. Cummins (2000), Fortnightly modulation of the estuarine circulation in Juan de Fuca Strait, *J. Mar. Res.*, *58*, 439–463.

Murray, C. P., S. L. Morey, and J. J. O'Brien (2001), Interannual variability of upper ocean vorticity balances in the Gulf of Alaska, *J. Geophys. Res.*, *106*, 4479–4491.

Penduff, T., B. Barnier, M.-A. Kerbiriou, and J. Verron (2002), How topographic smoothing contributes to differences between the eddy flows simulated by sigma- and geopotential coordinate models, *J. Phys. Oceanogr.*, *32*, 122–137.

Sarmiento, J. L., and K. Bryan (1982), An ocean transport model for the North Atlantic, *J. Geophys. Res.*, *87*, 394–408.

Smith, R. D., J. K. Dukowicz, and R. C. Malone (1992), Parallel ocean circulation modeling, *Physica D*, *60*, 38–61.

Smith, R. D., M. E. Maltrud, F. O. Bryan, and M. W. Hecht (2000), Numerical simulation of the north Atlantic ocean at 1/10°, *J. Phys. Oceanogr.*, *30*, 1532–1561.

Smith, W. H. F., and D. T. Sandwell (1997), Global sea floor topography from satellite altimetry and ship depth soundings, *Science*, *277*, 1956–1961.

Thompson, K. R., and E. Demirov (2006), Skewness of sea level variability of the world's oceans, *J. Geophys. Res.*, *111*, C05005, doi:10.1029/2004JC002839.

Thompson, K. R., D. G. Wright, Y. Lu, and E. Demirov (2006), A simple method for reducing seasonal bias and drift in eddy resolving ocean models, *Ocean Modell.*, *13*(2), 109–125.

Thomson, R. E., and J. F. R. Gower (1998), A basin-scale oceanic instability event in the Gulf of Alaska, *J. Geophys. Res.*, *103*, 3033–3040.

Woodgate, R. A., and P. D. Killworth (1997), The effects of assimilation on the physics of an ocean model. Part I: Theoretical model and barotropic results, *J. Atmos. Oceanic Technol.*, *14*, 897–909.

J. Shore and M. W. Stacey, Department of Physics, Royal Military College of Canada, Kingston, ON, Canada K7K 7B4. (stacey-m@rmc.ca)

K. R. Thompson, Department of Oceanography, Dalhousie University, Halifax, NS, Canada B3H 4J1.

D. G. Wright, Ocean Circulation Section, Bedford Institute of Oceanography, Dartmouth, NS, Canada B2Y 4A2.